Oxidation of *n*-Heptane in a Premixed Laminar Flame

Åsa T. Ingemarsson, Jörgen R. Pedersen, and Jim O. Olsson*

Department of Physical Chemistry, Chalmers University of Technology, SE-412 96 Göteborg, Sweden

Received: October 26, 1998; In Final Form: August 16, 1999

A premixed laminar *n*-heptane/air flame (1 atm and $\varphi = 1.0 \pm 0.05$) was investigated experimentally (using on-line GC/MS) and computationally. Ethene, propene, 1-butene, 1-pentene, 1-hexene, and 1-heptene showed broad peaks with maxima at a distance around 1000 μm from the burner. Methane, ethane, and propane showed more narrow peaks and maxima around 1075 μm. The following compounds with their maxima were found (mol %): ethene (0.99), methane (0.069), propene (0.127), ethyne (0.103), ethane (0.080), 1-butene (0.040), 1-pentene (0.021), and 1,3-butadiene (0.014). Concentrations of less than 0.01 mol % were detected for the components 1-heptene, propyne, propadiene, methanol, and acetaldehyde. The flame was modeled using the semiempirical mechanism by Held et al.[1] The model produced peaks of the organic intermediates at about 400−500 μm. Important measured species not present in the mechanism were propane, propyne, methanol, isobutene, 2-butene, and 1-heptene. The computed maxima of 1-butene, 1,3-butadiene, and 1-pentene were higher than the experimental maxima by a factor of about 2, 2, and 3, respectively. The model gives very similar results for two different pressures, 1 and 0.06 atm, except for a common scaling factor.

1. Introduction

Modern reformulated gasoline and high-quality diesel oil contains 70% and 95% alkanes, respectively. *n*-Heptane is suitable as a model compound in combustion investigations of *n*-alkanes.[1] It is also used as a primary reference fuel for octane rating in engines and has a cetane number similar to that for conventional diesel fuel.[2] Kinetic mechanisms for *n*-heptane have been developed for modeling of different combustion conditions: flow reactors, premixed flames, diffusion flames, and shock tubes.[1−5] These mechanisms are often used in computer modeling of combustors such as engines. Ignition, knocking, and emissions can be predicted. Modeling of combustion processes necessitates a very wide range of detailed experimental studies for evaluation/development of mechanisms. In a pioneering study, Hamins and Seshadri[6] measured the composition profiles of several species in a counterflow flame using on-line gas chromatography. However, there exist only a limited number of more detailed studies, with many organic compounds measured, of the pyrolysis/oxidation of *n*-heptane.[1,7,8] For example, only one detailed investigation of *n*-heptane in a premixed laminar flame has been performed (at low pressure).[8] More detailed experiments are necessary in order to evaluate and improve the combustion kinetic mechanisms further.

The goal of this study was to analyze the formation of stable organic compounds during combustion of *n*-heptane. A premixed laminar flame at stoichiometric composition burning at atmospheric pressure was investigated in detail using on-line GC/MS. The experimental results were compared with model predictions using a semiempirical mechanism developed by Held et al.[1]

2. Experimental Section

2.1. Fuel/Air Preparation. The gases were measured and controlled using a station constructed of Swagelock (Solon, OH) building blocks. The mixing station was equipped with HI-TEC F-201 mass flow meters/regulators connected to two four-channel controllers (Bronkhorst, Ruurlo, The Netherlands). A precision liquid chromatography pump, Rheos 4000 (Flux, Karlskoga, Sweden), delivered the liquid fuel. The pump exit was connected to a 3 m long polyetheretherketone (PEEK) tubing (0.13 mm i.d., 1.6 mm o.d. Alltech, Deerfield, IL) coupled to a heated line (Job-Tec, Stockholm, Sweden). The heated line contains inner inert (Teflon) tubing (6 mm i.d.). The temperature of the heated line was set to 180 °C. The pump delivered 70.0 μL/min of ±0.5% *n*-heptane, 99% pure (Kebo-Lab, Stockholm, Sweden), and the mixing station delivered 588 ± 10 mL/min dry air with 6 ± 0.30 mL/min krypton added. The krypton was used as an internal standard. In the heated line the liquid fuel was mixed with the gases coming from the mixing station. The gas flows were calibrated before each experiment using a DryCal DC-1 flow calibrator (BIOS, Pomton Plains, NJ). The liquid flow of *n*-heptane was calibrated by collecting the liquid flow for 10 min in a flask and then weighing the flask. The fuel/air ratio corresponded to an equivalence ratio of 1.0 ± 0.05.

2.2. Burner Setup. An atmospheric premixed burner, designed in-house and connected directly to the heated line above, was used. The burner consists of a stainless steel cylinder (30 mm height and 14 mm o.d.). To minimize the risk for flashback, two screens were placed inside the cylinder at different heights. These screens also induce a laminar flow of the fuel/air mixture. A thin (0.25 mm) disk (diameter 10 mm) made of stainless steel (Millipore, Bedford, MA) is clamped on top of the steel cylinder. The disk has a large number of holes (diameter 150 μm), evenly spaced over the surface, constituting about 40% of the area. The disk is exchanged with a new disk at the beginning of each experimental series. The burner produced

* To whom correspondence should be addressed. Fax: +46 31 772 38 58. E-mail: jim.olsson@phc.chalmers.se.

10.1021/jp984191s CCC: $18.00 © 1999 American Chemical Society
Published on Web 09/29/1999

premixed laminar (flat) flames. The small size of the burner obviates the need for extra cooling.

The burner is fastened on a motorized precision lift Stepper-Mike model 18503 with a precision of 1 μm (Oriel, Stratford, CT). A stepping motor controller (Oriel Stratford, CT) controlled the height of the lift. The burner/lift combination can be placed on top of or very close to the GC system with a minimum length of the sampling line.

A sampling microprobe[9] was positioned at the center of the flame. It consisted of a quartz capillary (13 cm length, 2 mm i.d., 3 mm o.d.) with a 0.1 mm inlet constriction in the tip. The tip of the capillary was shaped as a cone with a height of 3 mm and a top angle of about 30°. The microprobe was equipped with an air cooling assembly made of copper. The cooling assembly surrounded the microprobe above the tip. Changing the airflow through the cooling assembly varied the temperature of the probe. The airflow was set to create a temperature of 240 °C inside the tip of the probe.

2.3. Gas Sampling. The sampling microprobe was connected by polyetheretherketone (PEEK) sampling tubing and components (Alltech, Deerfield, IL) to a GC/MS system from HP (Hewlett-Packard, Palo Alto, CA).

First, the gas sample coming from the microprobe was connected to a $^1/_8$ in. male/male connector from Swagelock (Solon, OH). Teflon ferrules were used to fasten the quartz microprobe to the connector. An 80 mm long Silco steel tubing (1.0 mm i.d., 1.6 mm o.d.; Alltech, Deerfield, IL) protrudes 35 mm into the microprobe. The choice of this large diameter was made so that the restriction should be mainly in the tip of the probe. The Silco steel tubing was fastened to a Swagelock connector using $^1/_8$ to $^1/_{16}$ in. Teflon ferrules. The top of the Silco steel tubing was connected to a PEEK tubing, 120 cm (1.0 mm i.d., 1.6 mm o.d.; Alltech, Deerfield, IL). The tubing is connected via the GC-1 injection valve to the GC-1 sampling system. The injection valve was a Valco WT high-temperature (max temperature 325 °C) six-port two-position valve (Valco, Houston, TX) rotated by standard air pressure motor. The valve temperature was 250 °C. The sampling loop was made of stainless steel with a volume of 1 mL (1 mm i.d.). The injection mode was split/splitless. The size of the injection was determined by the time setting on the purge valve.

Pumping at the exit of the GC injection valve with various pumps resulted in peristaltic effects with increased sampling errors. The problem was circumvented by using a large vacuum vessel (25 L) kept at a constant pressure (30 mbar) by a SOGEVAC SV25 rotating pump (Leybold, Köln, Germany) connected to the vessel with a HI-TEC pressure controller system (Bronkhorst, Ruurlo, The Netherlands). The exit from the GC sampling valve was connected first to a restrictor consisting of a 75 cm length PEEK (0.5 mm i.d., 1.6 mm o.d.) tubing and then to another a fixed 3.5 m length PEEK (0.75 mm i.d., 1.6 mm o.d.) tubing. The longer tubing was connected directly to the vacuum vessel, and the length of the shorter tubing was chosen to yield a measured pumping rate of 50 $\pm$ 5 mL/min. This rate resulted in a maximum signal strength. The 0.5 mm i.d. PEEK tubing was kept at a constant temperature of 25 °C in a water bath. It is reasonable that the signal versus pumping rate should go through a maximum. When the pumping rate is zero, no sample reached the GC, and at high pumping rates the pressure in the sample loop becomes very low, resulting in a very small injection.

2.4. GC/MS System. In the GC/MS analysis a Hewlett-Packard (HP) 5890 series II GC connected to a HP 5989A MS engine (Palo Alto, CA) was used. The GC column was a PLOT fused-silica column 25 m $\times$ 0.25 mm (Chrompack, Middelburg, The Netherlands) with a coating of Poraplot Q. The carrier gas was hydrogen (99. 99999% pure) delivered by a hydrogen generator model 75-34 (Whatman, Maidstone, England). A HP Vectra 486/66N controlled the system. The software used was HP G1034C MS ChemStation rev A 03.03. The mass spectral library used for comparison/identification was Wiley 138 K provided by HP. Standards, liquids and gases, were available for some of the important compounds. The standards were injected into the systems in the same way as the sample from the flame. The compounds for which standards were not available were identified by use of the MS Wiley library. First, a GC method was developed by fixing the retention times for the different compounds (Table 1). Second, a selective ion monitoring (SIM) method was set up. The peaks have been integrated using the HP software. Generally, the integration accuracy is lower for minor components due to increased noise signal and more disturbances of baseline in the chromatograms. Furthermore, some of the components, for example, the C_4 species, are eluting as very narrow peaks in the chromatogram. However, this could be resolved by using the specific masses characteristic of the individual species. Formaldehyde was determined semiqualitatively using Supelclean Lp DNPH (dinitrohydrazine) S10 cartridges (Supelco, Bellefonte, PA).[10]

TABLE 1: GC/MS Setup

instruments and methods	configuration and values
instruments	HP 5890 series II GC HP 5989 A MS engine
column	Pora PLOT Q fused-silica 25 m $\times$ 0.25 mm i.d. 0.33 μm film
injection	manual gas injection Splitflow, 25 mL/min
injection port	250 °C
detector	MS (280 °C, SIM mode)
oven ramp	50 °C initial 3 min hold 20 °C/min to 130 °C 4 min hold 24 °C/min to 250 °C 2 min hold
flow rate	1 mL/min; H_2

The identification of the compounds was made either by using standards and/or by comparing mass spectra with a mass spectra library (Wiley 138K). Table 2 shows the method used for identification.

2.5. Quantification of Ion Peaks. To increase the sensitivity of the experiments, the SIM (selected ion monitoring) mode was used. The selected ions measured constituted only the largest mass fragments of the mass spectrum. The efficiency in collecting ions for a species using a specific SIM method will be decreased compared to the case that all the ions were collected. For a molecule m, the measured ion current, $I_{S,m}$, is a fraction, $S_{T,m}$, of the total ion current, $I_{T,m}$, obtainable. $S_{T,m}$ is defined as

$$S_{T,m} = \frac{I_{S,m}}{I_{T,m}} \tag{1}$$

To compute $S_{T,m}$ factors for a molecule m, the ratio of measured ions, according to the SIM method used, is divided by the total amounts of ions produced. The ratio factors, $S_{T,m}$, were computed using the averages of the spectra for the molecule, *m*, given in the MS library used (Wiley). Table 2 lists the S_T factor for the largest components found in the *n*-heptane flame.

TABLE 2: GC Retention Times and MS Factors Used for Quantification[a]

time (min)	name	Q	S_T	SIM
1.35	methane	4.432	0.471	16
1.39	krypton	3.50[b]	0.511	84
2.28	ethene	5.862	0.417	26
2.33	ethyne	4.402	0.764	26
2.79	ethane	7.322	0.538	26, 30, 31
5.84	propene#	8.752	0.560	39, 40, 41
6.07	propane	10.212	0.611	29, 30, 40, 41, 44
6.26	propadiene#	7.292	0.685	39, 40, 41
6.39	propyne#	7.292	0.730	39, 40, 41
7.16	methanol	5.532	0.862	29, 31
7.59	acetaldehyde	6.962	0.713	29, 41, 44
8.56	1-butene	11.642	0.704	39, 41, 54, 56
8.69	1, 3-butadiene	10.182	0.521	39, 54
8.93	isobutene	11.642	0.721	39, 41, 54, 56
9.12	2-butene#	11.642	0.699	39, 41, 54, 56
11.39	propanal#	9.852	0.128	42, 43, 55, 57
11.79	2-propanone	9.852	0.587	42, 43, 55, 57
12.56	1-pentene#	14.532	0.629	42, 55, 70
14.75	1-hexene	17.422	0.455	42, 43, 56, 57, 69
15.43	benzene	13.042	0.535	78
16.09	1-heptene	20.312	0.367	41, 56
16.10	*n*-heptane	21.772	0.378	42, 43, 56, 1000

[a] Q is the total electron ionization cross sections. S_t the ratio of ions collected and the total ions formed. SIM shows the selected ion peaks for use in selective ion monitoring. Normally, standards were used for identification. Species marked # were identified using the Wiley library. [b] Vallance et al., 1997.[13]

By use of eq 1 and an expression for the total ion current, $I_{T,m}$,[11] the measured ion current, $I_{S,m}$, can be expressed as

$$I_{S,m} = aI_e dS_{T,m} Q_m[X_m] \quad (2)$$

a is general apparatus properties expressing ion extraction, current amplification, etc., I_e is the ionization electron current, d is the ionization path length, Q_m is the total electron ionization cross section for the molecule m, and $[X_m]$ is the molar concentration of the molecule m.

Flame measurements are normally expressed as molar fractions. The mole fraction, X_m, is related to the molar concentration $[X_m]$ by[12]

$$X_m = (RT/p)[X_m] \quad (3)$$

where T is the flame temperature at that height, p is the pressure, and R is the universal gas constant. By use of eqs 2 and 3, the measured mole fraction X_m can be expressed by

$$X_m = \frac{F_a I_{S,m}}{S_{T,m} Q_m} \quad (4)$$

where $F_a = (RT/p)/(aI_e d)$ is function of temperature and therefore of the height z above the burner.

Finally, a small correction of the computed mole fraction concentration profiles was needed. During the combustion process there is a slight increase of 5% in the number of moles. At the burner surface the total molar flow was 27.0 mmol/min. At complete combustion, at a distance of 1 mm from the burner, the molar flow is 28.4 mmol/min. A linear correction of the mole fraction profiles between these two points was used.

2.6. Inert Internal Standards. In the experiments 1 ± 0.05 vol % krypton, i.e., $X_{Kr} = 0.010$, was added as an internal standard. The use of an inert gas as an internal standard allowed computation of the mole fraction profiles for the detected molecules. By use of $I_{S,Kr}$ measured at different heights z, F_a can be computed at corresponding heights from

$$F_a = S_{T,Kr} Q_{Kr} X_{Kr} / I_{S,Kr} \quad (5)$$

taking $S_{T,Kr}$ and Q_{Kr} from Table 2. By inserting in eq 3 the computed value of F_a at a specific height z, the mole fraction X_m for a specific molecule m can be computed at the same height.

The use of an internal standard corrects for general variations in the GC/MS instrument such as variations in GC injection and MS detection (decreased about 7%/h). Krypton elutes essentially undisturbed by other gases entering the MS ion source later than the nitrogen and oxygen. However, it was necessary to add krypton, since the concentration of krypton in air is only 1.14 ppm. This addition of krypton also allows the detection of flame disturbances, air leaks, etc. Such disturbances will increase the argon-to-krypton ratio.

2.7. Total Electron Ionization Cross Sections. It is necessary to use an additivity rule for computing Q_m the total electron ionization cross sections for the measured molecules. Fitch and Sauter[11] compared 179 sets of experimental cross sections for a range of organic molecules, m, and subjected these data to a multiple linear regression by using the numbers of each atom type as the independent variables. The resulting equation was

$$Q_m = 0.082 + \sum_{i=1}^{8} n_i a_i \quad (6)$$

where n_i is the number of atoms i in the molecule and a_i is the constant contribution coefficient of each atom type i (H, C, N, O, F, Cl, Br, and I) to Q_m, the molecular ionization cross section. The cross section coefficients used for C, H, and O were 1.43, 0.73, and 1.10, respectively. Fitch and Sauter[11] found a correlation coefficient of 0.996. Equation 6 was used to calculate the ionization cross sections of the hydrocarbons produced in the *n*-heptane/air flame. Table 2 lists the ionization cross sections used. The value for krypton was taken from an experiment by Vallance et al.[13] We also examined our method for computing ionization cross sections, using several different multicomponent gaseous and liquid standard mixtures. The difference compared to the additivity rule (eq 6) was within ±10% for the unsaturated hydrocarbons investigated. The oxygenates, methanol, MTBE, and acetone gave about 50% lower response compared to the additivity rule. Benzene, toluene, and xylene produced about 30%−40% lower response than the additivity rule predicted.

2.8. Temperature Measurements. The temperature of the burner disk was measured continuously during the experiments. A small (1 mm i.d.) thermocouple type K was positioned inside the burner in physical contact with the bottom side of the burner disk. The flame temperatures were measured using Pt−Pt/Rh10 thermocouples (0.10 mm i.d.) inserted in inert alumina tubes positioned parallel to the burner surface. Two thermocouples with different outer tube diameters d (0.5 and 1.0 mm) were used separately to determine the actual flame temperature. As expected, the coarse thermocouple showed consistently lower temperatures in comparison with the thin thermocouple. The radiation correction for these thermocouples, at a specific height z above the burner, depends on d, the outer tube diameter.[9] The actual flame temperature $T_{flame}(z)$ corresponds to the temperature measured if the outer diameter is infinitesimal $T_{0.0}(z)$. $T_{0.5}(z)$ is the measured temperature using the fine thermocouple, $T_{1.0}(z)$ is the measured temperature using the coarse thermocouple, and $T_{flame}(z)$ is the corrected flame temperature. $T_{flame}(z)$, the actual flame temperature, can be computed by

$$T_{\text{flame}}(z) \approx T_{0.5}(z) + (T_{0.5}(z) - T_{1.0}(z)) \quad (7)$$

The cooling in the sample point due to the cooled quartz microprobe was also investigated. A nude thermocouple, protruding out of an alumina thermocouple shielding tube, was positioned vertically in the microprobe holder. The temperature profiles were measured for three configurations relating to the cooling induced by the microprobe and its associated cooling assembly. First, we measured with the thermocouple bead about 4 mm from cooling assembly. This corresponds to the distance between the tip of the microprobe and the cooling assembly. Second, we measured the temperature profile with the bead 10 mm away from the cooling assembly. Third, we measured without the cooling assembly present. The measured temperature difference is a first-order approximation of the cooling of the sample introduced at the sampling point.

3. Numerical Modeling

The computations were performed using the Sandia flame code PREMIX.[14] The conditions inside the burner, at the burner surface, and close to the burner are very difficult to model. Therefore, the cold boundary conditions are simplified in the PREMIX flame code and other similar flame codes. For example, the burner is modeled as a cylinder with an open top surface without any obstructions. In reality, our burner is a metal disk with holes, with diameters of 150 μm, occupying about 40% of the area. Furthermore, in the flame code there are no surface reactions included. Consequently, the modeling results close to the burner are less reliable. This may result in a distortion of the length scale of the computational profiles compared to the experimental profiles.

The reaction mechanism of *n*-heptane oxidation and the associated thermochemical and transport data were taken from the work of Held et al.[1] The mechanism used consists of 266 reactions and 41 species. The reaction mechanism has been validated against flow reactor measurements, ignition delays, and laminar flame speeds.[1] However, it has not been used to predict the species profiles in laminar premixed flames. Krypton is present in only a minute inert amount in the combustible mixture. To simplify the computations, the krypton was treated as an extra addition of argon.

One major problem in the modeling of experimental flames is the uncertainty of the temperature history experienced by the sample. Molecules in a free adiabatic flame, a burner-stabilized flame (without cooling probe), and a burner-stabilized flame with a cooling probe represent the limiting cases. We have modeled a burner-stabilized flame with corrections included for the presence of a cooling probe. In the present study a corresponding base temperature profile was used. However, as discussed in many studies, the effect of the flame temperature on the sampled molecules may be very complex. Therefore, we also investigated the effect on species profiles of uncertainties in the temperature profile. The computations were performed using 10 different temperature profiles in the interval $\pm$200 K around the base temperature profile. As a complement, we modeled another heptane flame, also with $\phi = 1$ as in our experiment but burning at 0. 06 atm,[8] using the same reaction mechanism as above. During the final computations the values on the GRAD and CURVE parameters were 0.1 and 0.2, respectively. These values resulted in very dense grids of about 110 grid points situated mainly in the flame zones.

4. Results

4.1. GC/MS Measurements. The miniature flame reactor provided very good stability and reproducibility. A minimum of fuel is consumed compared to other types of reactors. Integration of a miniature flame reactor with an on-line GC/MS provided detailed chemical information on *n*-heptane combustion. The flame zone was narrow; the total flame height to burnout was 1.25 mm. We detected about 30 different stable organic intermediates. Figure 1 shows three chromatograms of the oxidation at 100, 1000, and 1300 μm from the burner surface. In the present experiment, taking place for 15 h, spurious electronic and flow disturbances will produce some outliers randomly. Table 3 shows examples of the reproducibility for the final run presented in this study. Figure 2 shows the resulting concentration profile of the *n*-heptane/air flame.

The species profiles of the C_2-C_7 alkenes formed; ethene, propene, 1-butene, 1-pentene, 1-hexene, and 1-heptene share a common form with broad peaks. Their concentration maxima were found at a distance around 1000 μm. Figure 3 shows the profiles for these compounds. Note that the ethene concentration is divided by 8 and that the propene concentration is divided by 2 in order to fit the profiles in the same plot. The species profiles of methane, ethane and, propane have a similar form with narrow peaks at around 1075 μm. Figure 4 shows the species profiles of methane, ethane, and propane. Note that the propane concentration is multiplied by 2. Alkynes and dienes (ethyne, propyne, propadiene, and 1,3-butadiene) have their maxima at around 1075 μm as the alkanes. Figure 5 shows profiles for alkynes and dienes. Note that the ethyne and 1,3-butadiene concentration is divided by 2 and that the propyne concentration is multiplied by 4. Methanol, acetaldehyde, 2-propanone, and propanal were also formed in the flame, and their profiles are shown in Figure 6. Note that the acetaldehyde concentration is divided by 2. The spatial averaging uncertainty due to the probe is estimated to be $\pm$50 μm. During the final experimental run the GC measurements were repeated at the distances of 500, 700, and 900 μm from the burner. These measurements illustrate the reproducibility during an experimental series (15 h). Some of these measurements are presented as double points in Figures 2−7 and also in Table 3.

Table 4 shows the major (20) organic intermediates measured. Dominating intermediate organic species were in decreasing order: ethene, propene, ethyne, ethane, methane, 1-butene, 1-pentene, propane, and 1,3-butadiene. For the concentration maxima note the pattern ethene > propene > 1-butene > 1-pentene > 1-hexene > 1-heptene. Alkene concentrations were found to be a factor 5−10 or higher than those of the corresponding alkanes. Significant amounts of propyne, propadiene, methanol, and acetaldehyde were also formed. The concentration of formaldehyde was found to be about 2−3 times higher than the acetaldehyde concentration. Traces of 2-propanone and propanal were also detected. Below the level of 2×10^{-03} mol % traces of higher hydrocarbons in the C_4-C_7 range were found: 2-alkenes, 3-alkenes, higher alkadienes, higher alkynes, and benzene. Most of these compounds showed very distributed profiles and only an approximate identification could be done for these. Figure 7 shows the species profiles of 2-butene, isobutene, and benzene, which are some of the minor organic intermediates, identified in the flame. Note that the benzene concentration is multiplied by 4.

4.2. Temperature Measurements. Figure 8 shows the temperature profile of the flame. The temperature on the bottom side of the burner disk was measured continuously during the experiments; the temperature was 550 $\pm$ 50 K. We believe that corrected flame temperatures at distances from 700 μm are

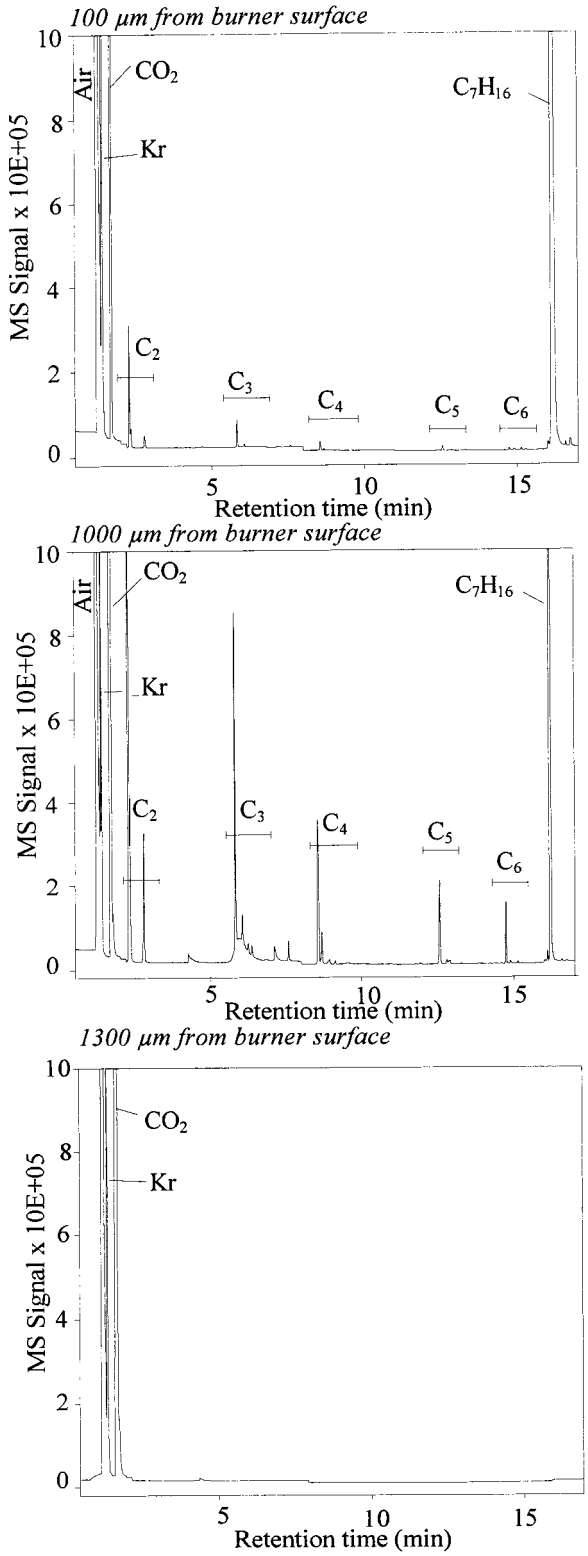

Figure 1. GC/MS chromatograms of the combustion products from a *n*-heptane/air premixed laminar flame burning at stoichiometric composition and atmospheric pressure. As an internal standard, 1 mol % krypton was added to the air. Chromatograms are at distances of 100 μm (top), 1000 μm (middle), and 1300 μm (below) from the burner surface.

accurate within ±150 K (see section 2.4). A further complication is introduced by local cooling at the sampling point due to the microprobe. We have determined the first-order effects of cooling at the sampling point. The presence of the cooling assembly was shown to decrease the temperature about 175 K.

TABLE 3: Reproducibilities of the GC/MS Measurements[a]

compound	500:1	500:2	700:1	700:2	900:1	900:2
ethene	0.516	0.510	0.649	0.657	0.791	0.794
methane	0.037	0.033	0.045	0.040	0.055	0.052
propene	0.082	0.080	0.102	0.104	0.120	0.124
ethyne	0.044	0.042	0.055	0.046	0.076	0.060
ethane	0.042	0.041	0.052	0.052	0.063	0.064
1-butene	0.026	0.026	0.033	0.035	0.038	0.040
1-pentene	0.014	0.014	0.017	0.018	0.020	0.021
propane	0.008	0.008	0.009	0.009	0.010	0.011
1.3-butadien	0.007	0.007	0.009	0.010	0.011	0.012
1-hexene	0.008	0.008	0.010	0.011	0.012	0.012

[a] Measured values, in mole percent, at three distances 500, 700, and 900 μm. The time between measurements 1 and 2 was about 10 h.

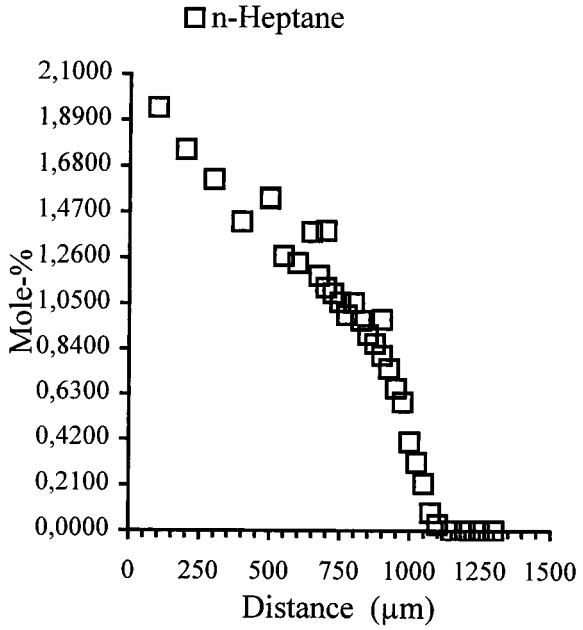

Figure 2. Concentration profile of *n*-heptane in a *n*-heptane/air flame. For conditions, see Figure 1 caption.

We also estimated that there is a small cooling of the quartz tip due to radiation corresponding to about 25 K.[9] In total, the presence of the cooled microprobe reduced the temperatures by at least 200 K at the sampling point. Recently, the cooling effect of the probe has been discussed and measured for an investigation of low-pressure *n*-heptane flames using a sampling cone.[8] The conclusion from their work is that the gas samples experience a complex temperature history composed of two effects, a maximum cooling close to the burner and a minimum cooling far from the burner.

4.3. Numerical Modeling. The temperature profile at the sampling points, corrected for cooling due to the cooled microprobe, was used as a base for the modeling (see Figure 8). Figure 9 shows the computational results, on a grid with 110 grid points, for the alkene intermediates. The locations of the concentration maxima of the species are shifted toward the burner in comparison with the present experimental study. The magnitudes of the maxima are with some exceptions within the uncertainties of the corresponding experimental values. An increase or decrease of the base temperature profile of 200 K shifted the location of the maxima about 0.02 cm toward or away from the burner, respectively. However, the maxima and especially the ratios of the maxima changed weakly with changes in the temperature profile. Table 5 shows the computational maxima using the two temperature profiles shown in Figure 8.

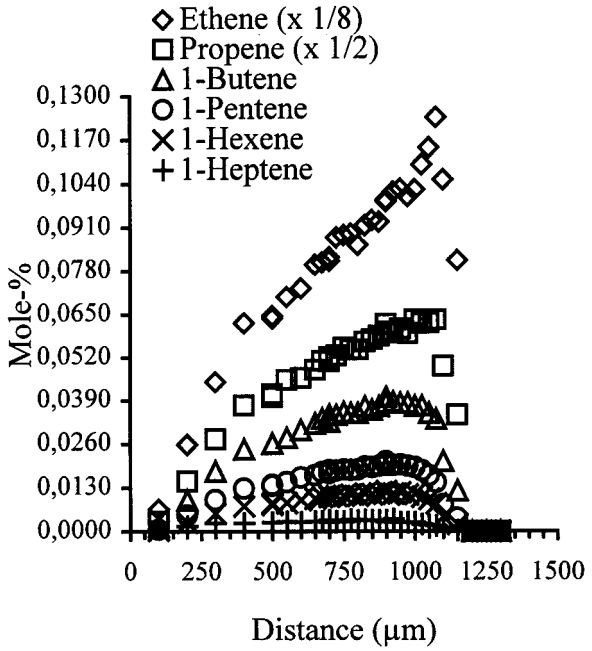

Figure 3. Concentration profiles of ethene, propene, 1-butene, 1-pentene, 1-hexene and 1-heptene in a *n*-heptane-air flame. Note that the ethene concentration is divided by 8 and that the propene concentration is divided by 2. For conditions, see Figure 1 caption.

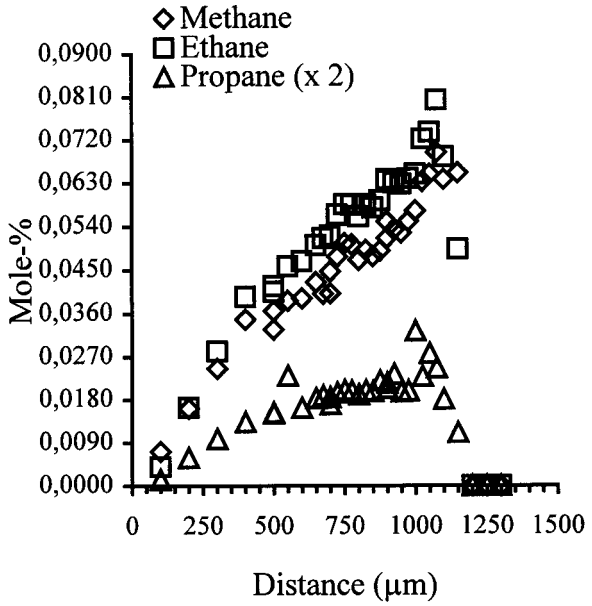

Figure 4. Concentration profiles of methane, ethane, and propane in a *n*-heptane/air flame. Note that the propane is multiplied by 2. For conditions, see Figure 1 caption.

Douté et al.[8] analyzed a low-pressure premixed laminar flame of *n*-heptane at a low pressure of 60 mbar and $0.7 < \varphi < 2.0$ using molecular beam mass spectrometry (MBMS) complemented by GC/MS for stable species. MBMS allows measurements of both stable species and free radicals. They observed a marked hierarchy in the concentrations of the intermediate alkenes measured. The maximum mole fractions decreased strongly with an increase in the carbon number, ethene > propene > 1-butene > 1-pentene. We modeled one of these low-pressure flames, also with $\phi = 1$ as in our experiment, using the same reaction mechanism as above. In most case, the experimental and modeling results agreed fairly well regarding

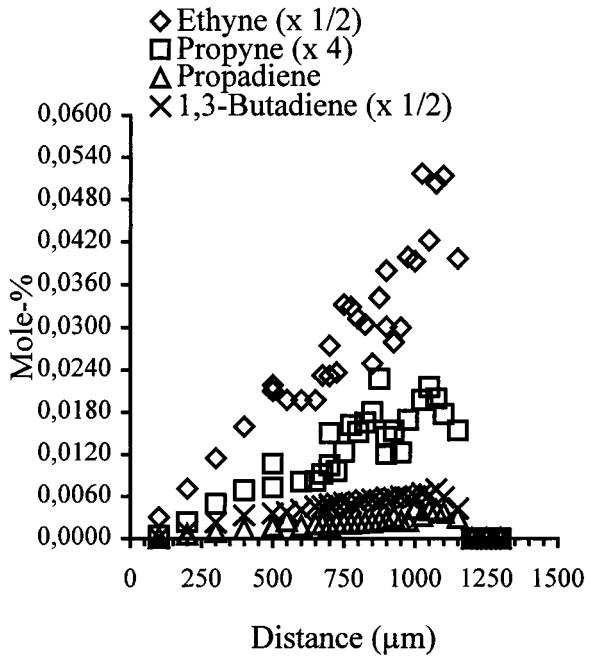

Figure 5. Concentration profiles of ethyne, propyne, propadiene, and 1,3-butadiene in a *n*-heptane/air flame. Note that the ethyne and 1,3-butadiene concentrations are divided by 2 and that propyne is multiplied by 4. For conditions, see Figure 1 caption.

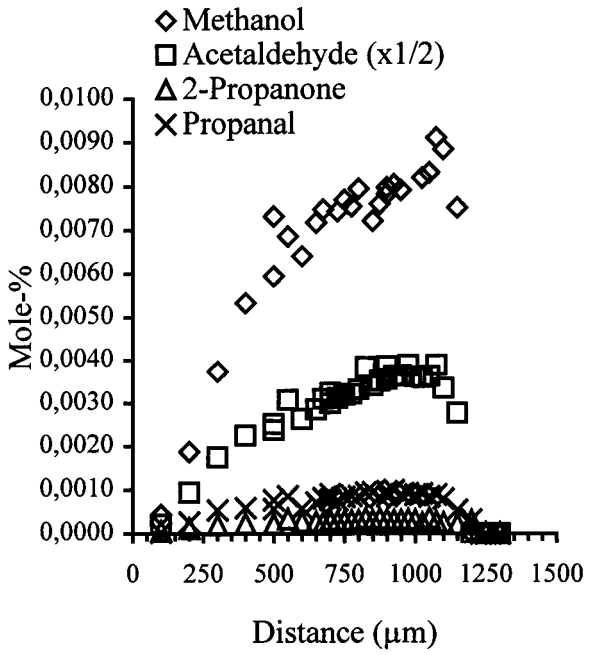

Figure 6. Concentration profiles of methanol, acetaldehyde, 2-propanone, and propanal in a *n*-heptane/air flame. Note that the acetaldehyde concentration is divided by 2. For conditions, see Figure 1 caption.

magnitude and locations of major stable organic intermediates. The modeling results showed analogous sensitivities to changes in the temperature profile as above. Table 6 shows the normalized computational results. In contrast to the model, Douté et al.[8] found that 1-pentene peaked at 0.05 cm from the burner. Then 1-butene, propene, and ethene peaks appeared at distances of 0.10, 0.20, and 0.245 cm from the burner, respectively. In comparison, the peaks of the same alkenes in the model are very compressed with positions between 0.130 and 0.165 cm.

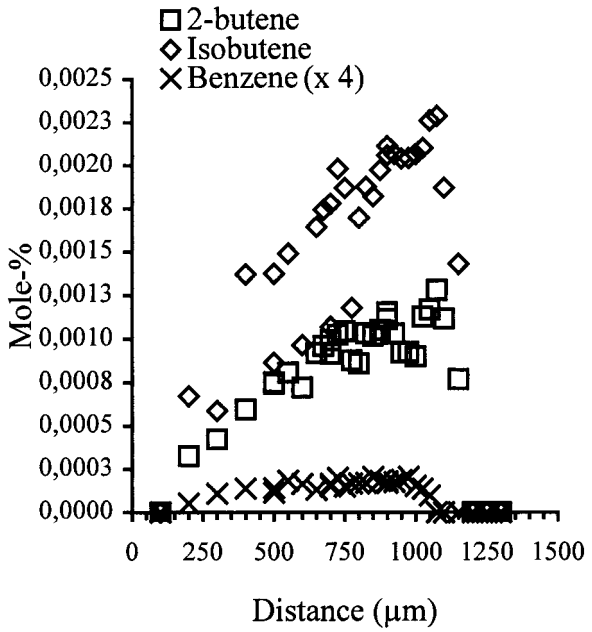

Figure 7. Concentration profile of 2-butene, isobutene, and benzene in a *n*-heptane/air flame. Note that the benzene concentration is multiplied by 4. For conditions, see Figure 1 caption.

TABLE 4: Organic Compounds Measured in the *n*-Heptane/Air Flame at $\varphi = 1$ and 1 atm[a]

name	distance (μm)	exptl max (mol %)
ethene	1075	0.990
propene	1000	0.127
ethyne	1025	0.103
ethane	1075	0.080
methane	1075	0.069
1-butene	900	0.040
1-pentene	900	0.021
propane	1000	0.016
1,3-butadiene	1075	0.014
1-hexene	900	0.012
methanol	1075	0.0091
acetaldehyde	1075	0.0078
propyne	875	0.0057
propadiene	1000	0.0042
1-heptene	925	0.0037
isobutene	1075	0.0023
2-butene	1075	0.0013
propanal	925	0.00099
2-propanone	1050	0.00036
benzene	850	5.0×10^{-5}

[a] Distances are estimated to be accurate within ± 50 μm. Species concentrations are uncertain by a factor of 1.5. Direct calibration indicated that the concentration maxima for the oxygenates should be a factor 2 higher. No corrections are made to the concentrations because of the calibration of the additivity rule (see section 2.7).

5. Discussion

First, we want to discuss the major concentration uncertainties involved in the present experiment. Second, we want to discuss our results in relation to other experiments and theoretical mechanisms.

5.1. Experimental Concentration Uncertainties. The present experimental setup is quite complex, which motivates a summary and discussion of the major uncertainties involved regarding concentration measurements. Several preliminary experimental series were produced, yielding consistent results. Most important, overlapping instrumental and evaluational methods regarding instrumental methods, internal standards, and calibration procedures were used. Therefore, the uncertainties could be minimized and checked subsequently.

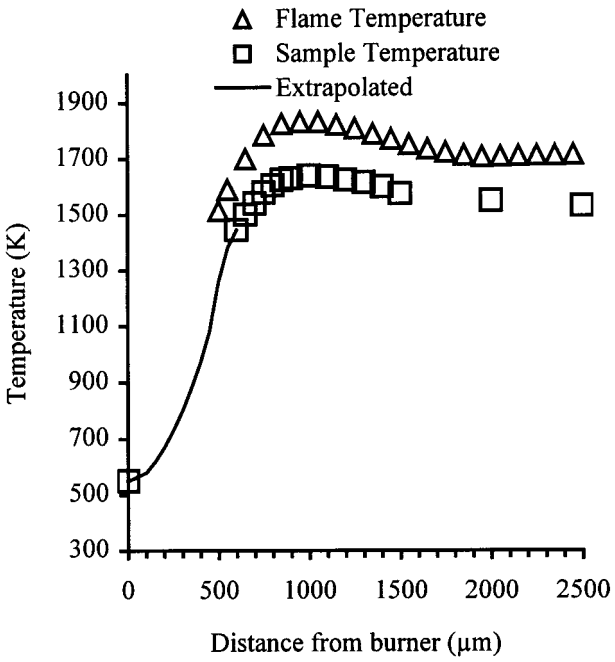

Figure 8. Flame temperature profile of the *n*-heptane/air flame. The line is an extrapolation of the temperature between 0 and 550 μm. For conditions, see Figure 1 caption.

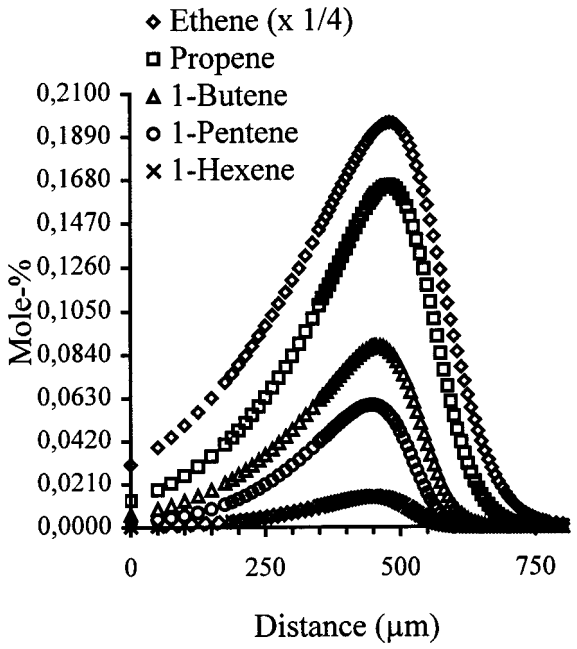

Figure 9. Computational results, on a grid with 110 grid points, for the alkene intermediates.

First, on-line GC/FID (aided by GC/FTIR for identification) as a complementary instrumental method was used. However, accurate absolute concentration measurements using a direct (inert) internal standard are not possible with GC/FID. The results, using the different GC methods, such as ratios of concentration maxima relative to ethene, were within $\pm 25\%$ in most cases. Second, to produce absolute concentration measurements, krypton was added as an internal standard. Use of an internal inert standard is the most reliable approach possible for quantification of signals to concentrations. The reason is that there are drifts in the experimental system and especially the GC/MS instrument. Use of a carbon mass balance does not

TABLE 5: Organic Compounds in the *n*-Heptane/Air Flame at $\varphi = 1$ and 1 atm[a]

	cooled probe		no probe	
name	dist (μm)	max (mol %)	dist (μm)	max (mol %)
ethene	481	0.783	356	0.697
propene	481	0.165	356	0.160
ethyne	563	0.184	444	0.142
ethane	444	0.097	331	0.113
methane	506	0.108	388	0.102
1-butene	456	0.088	331	0.111
1-pentene	447	0.060	331	0.063
1,3-butadiene	513	0.028	388	0.028
1-hexene	450	0.015	331	0.015
acetaldehyde	544	0.024	413	0.028
propadien	556	0.004	444	0.002
benzene	719	5×10^{-6}	519	3×10^{-6}

[a] Model predictions based on the mechanism by Held et al.[1] Temperature profiles used in the model were taken from Figure 8.

TABLE 6: Organic Compounds in the *n*-Heptane/Air Flame at $\varphi = 1$ and 0. 06 atm[a]

	experiment		model	
name	dist (cm)	max (mol %)	dist (cm)	max (mol %)
ethene	0.950	1.360	0.156	2.029
propene	0.200	0.450	0.163	0.480
ethyne	0.300	0.564	0.244	0.358
methane	0.250	unread	0.188	0.288
1-butene	0.100	0.152[b]	0.138	0.234
ethane		nd	0.119	0.305
1-pentene	0.050	0.061[b]	0.131	0.161
1,3-butadiene	0.250	0.034[b]	0.188	0.073
acetaldehyde		nd	0.250	0.072
1-hexene		nd	0.131	0.041
propadiene	0.250	0.007	0.231	0.008
benzene	0.300	7×10^{-4}	0.298	1×10^{-5}

[a] Experimental results by Douté et al. using MBMS.[8] [b] Calibrated by GC. MBMS gave higher values. Model predictions using the mechanism by Held et al.[1] and the temperature profile are from Figure 1c.[8]

work. Differential diffusion leads to changes in the elemental mass fraction for carbon atoms throughout a premixed laminar flame.[15]

Third, the determination of the final concentrations of the measured species was based on the use of the additivity rule for computing ionization cross sections. The good agreement with direct calibrations indicates that this was a good choice.

Fourth, the effect of nonlinearity was checked for several representative species including argon, krypton, methane, propane, heptane, and carbon dioxide. The major reason for nonlinearity is a temporary high pressure in the ion source. Only carbon dioxide, present at very high maximum concentrations, among the products showed a significant nonlinearity. For the HP 5989A MS engine, using powerful differential pumping, linearity of more than 3 orders of magnitude is expected.

We believe that the major uncertainty stems from integration of chromatographic peaks, especially small flat peaks disturbed by baseline noise. Overlapping of neighboring peaks is another factor increasing the concentration uncertainty. The results from the complementary methods discussed all produced consistent results. The concentration results presented here are uncertain by about a factor of 1.5 for the major intermediates.

5.2. Comparison with Other Reactor Experiments. Below we have cited experimental investigations of oxidation of *n*-heptane in different reactors.[1,7,8] Comparisons with other experimental studies are hampered by the fact that reproducibilities and uncertainties in concentration measurements are not normally well described or documented. In comparing these investigations, one has to understand some underlying similarities. The distance from a premixed laminar burner, the time in a flow reactor, and the temperature scale in a jet-stirred reactor experiment reflect the progress of the total reaction. Of course, there are also important differences. For example, the burner experiments are performed at higher temperatures, and transport effects affect the burner results. However, it is interesting to find out if there are features common for all of the investigations. Such features would reflect central properties in the oxidation of *n*-heptane, independent of the specific physical condition and specific reactor.

Held et al.[1] investigated lean and rich oxidation of *n*-heptane in a flow reactor at 3 atm and a temperature interval between 930 and 980 K. The intermediate organic species consisted primarily of small alkenes in decreasing quantity as the carbon number increased. The largest alkene detected was 1-hexene (limit, 1−5 ppm); errors and reproducibilities were not given. C_4-C_6 species formed early in the reaction, ethane formed in the middle of the reaction, and the other C_1-C_3 species formed relatively late. An exception to the rule was 1,3-butadiene, which formed late in the reaction. Interestingly, Held et al.[1] found that, in comparison with experiment, for $\varphi = 0.79$ the model produced a factor of 2.5 higher maximum of 1-pentene than the experiment. For 1-butene and 1,3-butadiene the model produced a factor of 1.5 higher maxima than the experiment. Dagaut et al.[7] investigated oxidation of *n*-heptane in a jet-stirred reactor (550−1150 K, 10 atm, $0.3 \leq \varphi \leq 1.5$). For the alkenes the highest maximum mole fractions were found for ethene > propene > 1-butene > 1-pentene > 1-hexene. Other intermediate hydrocarbons at high concentrations were methane, ethane, and 1,3-butadiene. C_4-C_7 species formed at low temperatures, ethane formed at intermediate temperatures, and the other C_1-C_3 formed at higher temperatures. The dominating oxygenates found were formaldehyde, acetaldehyde, methanol, propanal, and 2-propanone.

There are four central features found in our study and supported by the experimental investigations discussed above.[1,7,8] They exhibit the same following key features as our study. First, there is a marked hierarchy in the maxima of the species profiles in the concentrations of the intermediate alkenes: ethene > propene > 1-butene > 1-pentene >1-hexene > 1-heptene. Second, the concentrations of the alkenes are significantly higher than the corresponding alkanes. Third, C_4-C_7 intermediates peaks early during the oxidation of *n*-heptane and C_1-C_3 hydrocarbons late. Fourth, as an exception to the rule, 1,3-butadiene forms late. Strikingly, the key features above are true over a wide range of φ (equivalence ratio) and pressure.

5.3. Differences between Computational and Experimental Concentration Maxima. In the present study we have investigated a flame model based on the semiempirical mechanism developed by Held et al.[1] The most important results are summarized in Table 7. The model describes the produced amount of major organic intermediates comparatively well. However, important species not present in the mechanism are propane, propyne, methanol, isobutene, 2-butene, and 1-heptene. Therefore, the model will have a reduced flexibility. Furthermore, compared to the present flame experiment the model produced significantly higher maxima for some species: 1-butene, 1,3-butadiene, and 1-pentene. Similar results, regarding 1,3-butadiene and 1-pentene, for the low-pressure flame experiments measured by Douté et al.[8] at $\varphi = 1$ were found. Furthermore,

TABLE 7: Organic Compounds in the *n*-Heptane/Air Flames at $\varphi = 1$[a]

name	expt 1 atm	model 1 atm	expt 0.06 atm	model 0.06 atm
ethene	1	1	1	1
propene	0.128	0.210	0.331	0.237
ethyne	0.104	0.236	0.415	0.176
methane	0.070	0.139	unread	0.142
1-butene	0.040	0.112	0.118	0.115
ethane	0.081	0.124	nd	0.150
1-pentene	0.021	0.076	0.045	0.079
1,3-butadiene	0.014	0.036	0.025	0.036
acetaldehyde	0.008	0.030	nd	0.035
1-hexene	0.012	0.019	nd	0.020
propadien	0.004	0.005	0.005	0.004
benzene	5×10^{-5}	6×10^{-6}	5×10^{-4}	5×10^{-6}

[a] Normalized maximum values for organics with respect to ethene, based on Tables 4−6. Present experiment at 1 atm and experiment at 0.06 atm by Douté et al.[8] using MBMS. Model predictions are based on the mechanism by Held et al.[1]

in a flow reactor Held et al.[1] themselves found significant higher computational maxima compared to their experimental concentration maxima, for 1-butene, 1-pentene, and 1,3-butadiene for the lean case at $\varphi = 0.79$. The flame model also produced a factor of 10 less benzene compared to the present experiment. For the low-pressure experiments[8] at $\varphi = 1$ the model produced a factor of 100 less benzene than the experiment. Normalization against ethene revealed that for the stoichiometric conditions evaluated, the mechanism behaved very similarly, within a wide range of temperatures of ±200 K for two very different pressures 1 and 0.06 atm (see Table 7). For a recent explanation of such scaling effects with pressure, see Pope et al.[15] The breakdown, resulting in subsequent formation of a sequence of gradually smaller alkenes, is very compressed in the model in comparison with the experimental results obtained at 0.06 atm by Douté et al.[8]

The central features of high-temperature oxidation of *n*-heptane are as follows.[1,2] H abstraction of *n*-heptane leads to formation of four distinct *n*-heptyl radicals 1-heptyl, 2-heptyl, 3-heptyl, and 4-heptyl. Site-specific abstraction rate constants control the formation rates of 1-alkenes. Because of the ethene, propene, 1-butene, 1-pentene, and 1-hexene will form in decreasing amounts. The smaller alkenes such as ethene will also form via other reactions paths. In the semidetailed mechanism used in the present study, this complex initial oxidation of *n*-heptane is compressed in a few empirical reactions. Furthermore, many important organic intermediates are not present in the present simplified mechanism. The high computational concentration maxima found, compared to the experiments, with regard to 1-butene, 1-pentene and 1,3-butadiene may be explained by these simplifications. For the case of 1,3-butadiene, Held et al.[1] stated that the discrepancy found in their oxidation experiment was probably due to an incomplete oxidation mechanism. However, the combined effect of the uncertainties of the rate constants in a flame model may also lead to distortions of the computed maxima. This is best illustrated by comparing two different heptane mechanisms. For example, for $\phi = 1.3$ the computed flame velocities are 29.4 and 45.7 cm/s using the flame models developed by Held et al.[1] and Lindstedt and Maurice,[3] respectively. This is a very substantial difference indicating significant uncertainties regarding central parameters in one or both of the flame models.

Acknowledgment. We are very grateful to Prof. Dryer and Dr. Kosakov at Princeton University for sending us their mechanism and preliminary results regarding heptane flames. This work was in part supported by the Combustion Engine Research Center, Chalmers University of Technology, Bycosin AB, Karlstad and Kemiindustrins forskarskola, Association of Swedish Chemical industries, Stockholm.

References and Notes

(1) Held, T. J.; Marchese, A. J.; Dryer, F. L. *Combust. Sci. Technol.* **1997**, *123*, 107−146.

(2) Curran, H. J.; Gaffuri, P.; Pitz, W. J.; Westbrook, C. K. *Combust. Flame* **1998**, *114*, 149−177.

(3) Lindstedt, R. P.; Maurice, L. Q. *Combust. Sci. Technol.* **1995**, *107*, 317−353.

(4) Bollig, M.; Pitsch, H.; Hewson, J. C.; Seshadri, K. *Twentysixth Symposium (International) on Combustion*; Combustion Institute: Pittsburgh, PA, 1996; pp 729−737.

(5) Come, G. M.; Warth, V.; Glaude, P. A.; Fournet, R.; Battin-Leclerc, F.; Scacchi, G. *Twentysixth Symposium (International) on Combustion*; Combustion Institute: Pittsburgh PA, 1996; pp 755−762.

(6) Hamins, A.; Seshadri, K. *Combust. Flame* **1987**, *68*, 295−307.

(7) Dagaut, P.; Reuillon, M.; Cathonnet, M. *Combust. Sci. Technol.* **1994**, *95*, 233−260.

(8) Douté, C.; Delfau, J. L.; Akrich, R.; Vovelle, C. *Combust. Sci. Technol.* **1997**, *124*, 249−276.

(9) Fristrom, R. M.; Westenberg, A. A. *Flame Structure*; McGraw-Hill Inc.: New York, 1965.

(10) Ingemarsson, Å.; Nilsson, U.; Nilsson, M.; Pedersen, J.; Olsson, J. *Chemosphere* **1998**, *36*, 2879−2889.

(11) Fitch, W. L.; Sauter, A. D. *Anal. Chem.* **1983**, *55*, 832−835.

(12) Kee, R. J.; Miller, J. A.; Jefferson, T. H. Report SAND80-8003; Sandia National Laboratories: Livermore, CA, 1980.

(13) Vallance, C.; Harris, S. A.; Hudson, E. J.; Harland, P. W. *J. Phys. B* **1997**, *30*, 2465−2475.

(14) Kee, R. J.; Grcar, J. F.; Smooke, M. D.; Miller, J. A. *A Fortran Program for Modeling Steady Laminar One-Dimensional Premixed Flames*; Report SAND85-8240; Sandia National Laboratories: Livermore, CA, 1985.

(15) Pope, C. J.; Shandross, R. A.; Howard, J. B. *Combust. Flame* **1999**, *116*, 605−614.